AGU PUBLICATIONS

Water Resources Research

RESEARCH ARTICLE
10.1002/2015WR017558

Companion to
*Razavi and Gupta* [2016],
doi:10.1002/2015WR017559.

**Key Points:**
- The VARS framework enables sensitivity analysis across a full range of scales
- Sobol and Morris are special cases of the VARS framework
- VARS is highly efficient because it utilizes information from pairs of points

**Correspondence to:**
S. Razavi,
saman.razavi@usask.ca

**Citation:**
Razavi, S., and H. V. Gupta (2016), A new framework for comprehensive, robust, and efficient global sensitivity analysis: 1. Theory, *Water Resour. Res.*, *52*, 423–439, doi:10.1002/2015WR017558.

Received 14 MAY 2015
Accepted 10 DEC 2015
Accepted article online 15 DEC 2015
Published online 28 JAN 2016



# A new framework for comprehensive, robust, and efficient global sensitivity analysis: 1. Theory

**Saman Razavi[1,2] and Hoshin V. Gupta[3]**

[1]Global Institute for Water Security & School of Environment and Sustainability, University of Saskatchewan, Saskatoon, Saskatchewan, Canada, [2]Department of Civil and Geological Engineering, University of Saskatchewan, Saskatoon, Saskatchewan, Canada, [3]Department of Hydrology and Water Resources, University of Arizona, Tucson, Arizona, USA

**Abstract** Computer simulation models are continually growing in complexity with increasingly more factors to be identified. Sensitivity Analysis (SA) provides an essential means for understanding the role and importance of these factors in producing model responses. However, conventional approaches to SA suffer from (1) an ambiguous characterization of sensitivity, and (2) poor computational efficiency, particularly as the problem dimension grows. Here, we present a new and general sensitivity analysis framework (called VARS), based on an analogy to "variogram analysis," that provides an intuitive and comprehensive characterization of sensitivity across the *full spectrum of scales* in the factor space. We prove, theoretically, that Morris (derivative-based) and Sobol (variance-based) methods and their extensions are special cases of VARS, and that their SA indices can be computed as by-products of the VARS framework. Synthetic functions that resemble actual model response surfaces are used to illustrate the concepts, and show VARS to be as much as two orders of magnitude more computationally efficient than the state-of-the-art Sobol approach. In a companion paper, we propose a practical implementation strategy, and demonstrate the effectiveness, efficiency, and reliability (robustness) of the VARS framework on real-data case studies.

## 1. Background and Objective

Computer simulation models are essential components of research, design, development, and decision-making in science and engineering. With continuous advances in understanding and computing power, such models are becoming more complex with increasingly more factors to be specified (model parameters, forcings, boundary conditions, etc.). To facilitate better understanding of the role and importance of different model factors in producing model responses, the procedure known as "Sensitivity Analysis" (SA) can be very helpful.

The SA-related literature is quite large, discussing the development of various approaches to SA and their widespread application to a variety of simulation models [see *Razavi and Gupta*, 2015 and references therein]. However, as outlined in *Razavi and Gupta* [2015], two issues continue to pose major challenges:

1. Ambiguous Characterization of Sensitivity: different SA methods are based in different philosophies and theoretical definitions of sensitivity. The absence of a *unique* definition for sensitivity can result in different, even conflicting, assessments of the underlying sensitivities for a given problem.
2. Computational Cost: the cost of carrying out SA can be large, even excessive, for high-dimensional problems and/or computationally intensive models. This cost varies significantly for different methods, where cost (or "efficiency") is commonly assessed in terms of the number of samples (model simulation runs) required for the method to generate statistically robust and stable results.

This set of companion papers presents a theoretical and practical framework for addressing the above mentioned dual aspects of effectiveness and efficiency. By "effective" we mean achieving an assessment that is both meaningful and clearly reflective of the objective of the analysis (the first challenge above), while by "efficient" (or economical) we mean achieving statistically robust results with minimal computational cost (the second challenge above). Based on this approach, we develop a "global" sensitivity analysis framework that generates a set of sensitivity indices that characterize important properties of "response surfaces"

encountered when performing SA on computer simulation models. Further, we show how this framework embraces, and is consistent with, a spectrum of different concepts regarding "sensitivity," while reducing to certain commonly used SA approaches under specific conditions.

In *Razavi and Gupta* [2015], we identified several important sensitivity-related characteristics of response surfaces that must be considered when investigating and interpreting the "global sensitivity" of a model response (e.g., a metric of model performance) to its parameters/factors. These include:

a. Local sensitivities (i.e., first-order derivatives),
b. Global distribution of local sensitivities (characterized, for example, by their mean and variance, or by some other statistics),
c. Global distribution of model responses (characterized, for example, by their variance, or by some other statistics), and
d. Structural organization (shape) of the response surface (including its multi-modality and degree of non-smoothness/roughness).

Existing global sensitivity analysis (GSA) approaches typically focus on only *one* or *two* of these characteristics while ignoring the others. Also, the methods that focus on properties (a) and (b) above are prone to the "scale" issue, so that their conclusions regarding relative sensitivity of different factors depend on the step size used in the numerical calculation of local sensitivities.

01 mingxi zhang

Because the Sobol and Morris approaches (and their extensions) provide the most rigorous approaches to GSA to-date, we use them as benchmarks against which to demonstrate our framework. The Sobol approach [*Homma and Saltelli*, 1996; *Sobol'*, 1990] is based entirely on the global distribution of model responses (characteristic (c) above), decomposing the global variance of model response into components associated with individual contributing factors. As such, the Sobol approach is unable to distinguish between response surfaces that have identical variance (or distribution) but different structures (spatial organizations) and/or derivative distributions. On the other hand, the Morris approach [*Morris*, 1991], and its various extensions [*Campolongo et al*., 2007; *Sobol and Kucherenko*, 2009], focus only on the global distribution of local sensitivities (characteristic (b) above) and provide globally aggregated assessments of the contributions of individual factors to distributional properties of local sensitivities. *Razavi and Gupta* [2015] provide a critical assessment of the Sobol and Morris approaches and demonstrate and discuss their strengths and shortcomings.

02 mingxi zhang

The new framework presented in this paper provides a platform to encompass the four sensitivity-related characteristics of response surfaces, while directly addressing the scale issue.

The paper is organized as follows. Section 2 presents the theoretical basis for our proposed framework for SA, illustrates it via simple conceptual examples, and proposes a summary metric suitable for characterizing factor sensitivity in *Earth and Environmental System Models* (EESMs) and beyond. In section 3, we derive the *theoretical relationship* between our approach and the commonly used "derivative-based" Morris and "variance-based" Sobol approaches. Section 4 explains how the new framework can characterize structural properties of response surfaces such as small-scale fluctuations or large-scale modes. Section 5 demonstrates the *effectiveness* and *efficiency* of our proposed framework on a synthetic six-dimensional response surface. Section 6 summarizes and discusses the contributions of this paper. In the companion paper, *Razavi and Gupta* [2016], we discuss and illustrate the practical numerical implementation and application of the new framework to real-world problems.

## 2. Theoretical Development

Our approach to sensitivity analysis is based on an analogy to "Variogram Analysis." Variograms are powerful tools for characterizing the spatial (or spatiotemporal) structure and variability of a dependent variable (e.g., a model response) across the space formed by a set of factors. In the context of computer simulation models, this is analogous to a characterization of the "response surface" of a model, which represents how a target response (a state or output variable, or a performance metric) varies with one or more factors of interest. We use the term "factor" to indicate any feature of a model (e.g., its parameters, forcings, boundary conditions, etc.) that can vary across a continuous, discrete, or hybrid domain that defines the "factor space."

Suppose that the response of a model is represented by function $f$ as:

$$y=f(x_1,\ \ldots,\ x_n) \tag{1}$$

where $x_1,\ \ldots,\ x_n$ are factors of interest varying within a space defined by the $n$-dimensional hypercube bounded between $x_1^{\min},\ \ldots,\ x_n^{\min}$ and $x_1^{\max},\ \ldots,\ x_n^{\max}$. We seek to characterize the "global sensitivity" of $y$ with respect to $x_1,\ldots, x_n$. In adopting the variogram concept, we make the assumption that the model response surface can be treated as though it is a realization of a stochastic process. This assumption is clearly reasonable since any model response, such as a Mean Squared Error (MSE) or Maximum Likelihood Estimator (MLE) performance metric, is subject to stochastic variation due to numerous factors (including model structural inadequacies, parameter uncertainties, data errors, and data period selection).

### 2.1. Variogram Analysis of Response Surfaces (VARS)

In the field of spatial statistics, a variogram is a function that characterizes the spatial covariance structure of a stochastic process. It is defined as the variance of the differences between response surface values computed at (a large number of) pairs of points at different locations across the factor space.

Let $\boldsymbol{x}=\{x_1,\ \ldots,\ x_n\}$ represent a location in the $n$-dimensional factor space, and $A$ and $B$ be two points with locations $\boldsymbol{x}^A$ and $\boldsymbol{x}^B$. Then, for the response surface represented by equation (1) we have:

$$E(y(\boldsymbol{x}))=\mu_y \tag{2}$$

$$V\left(y\left(\boldsymbol{x}^A\right)-y\left(\boldsymbol{x}^B\right)\right)=2\gamma\left(\boldsymbol{x}^A-\boldsymbol{x}^B\right) \tag{3}$$

$$COV\left(y\left(\boldsymbol{x}^A\right),y\left(\boldsymbol{x}^B\right)\right)=C\left(\boldsymbol{x}^A-\boldsymbol{x}^B\right) \tag{4}$$

where $E$, $V$, and $COV$ represent expected value, variance, and covariance, respectively, and $\gamma(.)$ and $C(.)$, called a "variogram" and a "covariogram," respectively, are functions of only the increment $\boldsymbol{x}^A-\boldsymbol{x}^B$. Equation (2) is known as the "constant mean assumption." A stochastic process satisfying equations (2) and (3) is said to be "intrinsic stationary" and when satisfying equations (2) and (4) is said to be "second-order or wide-sense stationary." Notably, the class of second-order stationary processes is strictly contained in the class of intrinsic stationary processes. For details regarding these assumptions, see *Cressie* [1993].

Defining $\boldsymbol{h}=\boldsymbol{x}^A-\boldsymbol{x}^B$ so that $\boldsymbol{h}=\{h_1,\ h_2,\ \ldots,\ h_n\}$, we can write the "multidimensional variogram" as:

$$\gamma(\boldsymbol{h})=\frac{1}{2}V(y(\boldsymbol{x}+\boldsymbol{h})-y(\boldsymbol{x})) \tag{5}$$

and under the constant mean assumption (intrinsic stationary process), this becomes:

$$\gamma(\boldsymbol{h})=\frac{1}{2}\ E\left[(y(\boldsymbol{x}+\boldsymbol{h})-y(\boldsymbol{x}))^2\right] \tag{6}$$

For any response surface having a closed-form functional expression, the multidimensional variogram can be analytically derived as:

$$\gamma(\boldsymbol{h})=\frac{1}{2D}\int_{\Omega}(y(\boldsymbol{x}+\boldsymbol{h})-y(\boldsymbol{x}))^2\ d\boldsymbol{x} \tag{7}$$

where $\int_{\Omega}(.)\ d\boldsymbol{x}$ represents a multiple integral over the factor space such that $d\boldsymbol{x}=dx_1\ldots dx_n$, $\Omega=\left[x_{i=1:n}^{\min},\ x_{i=1:n}^{\max}-h_{i=1:n}\right]^n$, and $D=\prod_{i=1}^{n}\left(x_i^{\max}-x_i^{\min}\right)$. The variogram (equation (6)) is classically estimated by sampling $y(\boldsymbol{x})$ at a number of locations, $\boldsymbol{x}$, across the domain of the factor space so that:

$$\gamma(\boldsymbol{h})=\frac{1}{2|\mathrm{N}(\boldsymbol{h})|}\sum_{(i,j)\in\mathrm{N}(\boldsymbol{h})}\left(y\left(\boldsymbol{x}^A\right)-y\left(\boldsymbol{x}^B\right)\right)^2 \tag{8}$$

where $\mathrm{N}(\boldsymbol{h})$ denotes the set of all possible pairs of points $\boldsymbol{x}^A$ and $\boldsymbol{x}^B$ in the factor space, such that $|\boldsymbol{x}^A-\boldsymbol{x}^B|=\boldsymbol{h}$, and $|\mathrm{N}(\boldsymbol{h})|$ is the number of pairs in that set.

To assess factor sensitivity, we are interested in the covariance structures along the direction of each of the factors. Accordingly, "Directional Variograms" are of particular interest, where the directional variogram

$\gamma(h_i)$ with respect to the $i^{th}$ factor is a one-dimensional function, equivalent to $\gamma(\boldsymbol{h})$ when $h_j=0$ for all $j \neq i$. We demonstrate in section 2.2 how directional variograms characterize useful information regarding the sensitivity of the response surface to each of the factors. They form the building blocks of our proposed framework for SA, which we call "Variogram Analysis of Response Surfaces" or the VARS framework.

When the underlying stochastic process is assumed to be *isotropic* (invariant with respect to direction), the variogram can be represented as a one-dimensional function of the distance $\|\boldsymbol{h}\|$ that indicates the length of vector $\boldsymbol{h}$. We refer to this variogram, denoted by $\gamma(\|\boldsymbol{h}\|)$, as the "Overall Variogram." Note that, when applied to function response surfaces, the overall variogram characterizes some average, nondirectional covariance, and can therefore be used to normalize the directional variograms and resulting VARS-based sensitivity metrics.

### 2.2. Illustration Using Conceptual Examples

#### 2.2.1. Points to Pairs: Numerical Calculation of Variograms and Covariograms

A simple, hypothetical response surface is utilized to show how variogram $\gamma(h)$ and covariogram $C(h)$ of a response surface can be derived from samples of points on the response surface. Figure 1a shows this one-factor response surface with 10 randomly sampled points. Figures 1c and 1e show how the individual samples of the response surface are mapped (as pairs of samples) onto the variogram and covariogram spaces. As shown, the 10 sampled points result in 45 pairs of points with a wide range of $h$ values (from 0.02 to 0.93). As a more comprehensive example, Figure 1b shows 50 regularly spaced points sampled from the response surface, which result in a total of 1225 pairs mapped onto Figures 1d and 1f. Averaging the clouds of points (in the vertical direction for each $h$ value) on the plots yields the variogram/covariogram.

The following points are of significance:

1. The number of pairwise combinations from a given set of $k$ sampled points is $k!/2!(k-2)!=k(k-1)/2$. In this example, the 5-fold increase in the number of sampled points (from 10 to 50) results in a 27-fold increase in the number of pairs.
2. The covariogram $C(h)$ in this example tends towards the variance $V(y)$ in the limit as the pairwise distance $h$ approaches zero (i.e., $C(h) \rightarrow V(y)$ when $h \rightarrow 0$). This important behavior and its relevance will be discussed in section 3.2.

#### 2.2.2. Variogram Relation to Sensitivity

In the VARS framework, we interpret variograms as a comprehensive manifestation of sensitivity information. To this end, VARS links variogram analysis to the important concepts of "direction" and "scale." Based in fundamental properties of variograms, we define that a higher value of $\gamma(h_i)$ for any given $h_i$, indicates a higher "rate of variability" (or "sensitivity") of the underlying response surface in the *direction* of the $i^{th}$ factor, at the *scale* represented by that $h_i$ value. Notably, this rate of variability at a particular scale in the problem domain represents the "scale-dependent sensitivity" of the response surface to the corresponding factor. Because variograms are defined over the full range of scales, they provide a spectrum of information about the sensitivity of the model response to the factor of interest.

To demonstrate and clarify the relation of variograms to sensitivity (the fundamentals of the VARS concept), we use the simple examples 1a–1c (shown in Figure 2) adopted from *Razavi and Gupta* [2015]. In these examples, the benchmark Sobol approach is represented by the variance of the response surface, $V(y)$, and the Morris approach is represented by the averages of absolute and squared local sensitivities across the factor range, $E\left(\left|\frac{dy}{dx}\right|\right)$ and $E\left(\left(\frac{dy}{dx}\right)^2\right)$. Note that in these examples, we are able to compute the derivatives analytically, whereas in real-world case studies the derivatives $\frac{dy}{dx}$ are usually estimated numerically by $\frac{\Delta y}{\Delta x}$ [see *Morris*, 1991], where the step size $\Delta x$ in the factor space is analogous to $h$ in the VARS approach.

***Example 1a: Unimodal functions with different structures.*** Figure 2a presents three unimodal functions (each having a single unique minimum) of the kind shown in optimization textbooks. Based on the derivative functions shown in Figure 2b, $E\left(\left|\frac{dy}{dx}\right|\right)=a$ for all three functions, $E\left(\left(\frac{dy}{dx}\right)^2\right)=\frac{4a^2}{3}$ for functions $f_1$ and $f_3$, and $E\left(\left(\frac{dy}{dx}\right)\right)^2=a^2$ for function $f_2$. In addition, the overall variance $V(y)=\frac{4a^2}{45}$ for functions $f_1$ and $f_3$, and their probability density functions (PDFs) are mirror images of each other (see Figure 2c). Meanwhile, the variance $V(y)=\frac{a^2}{12}$ for function $f_2$.

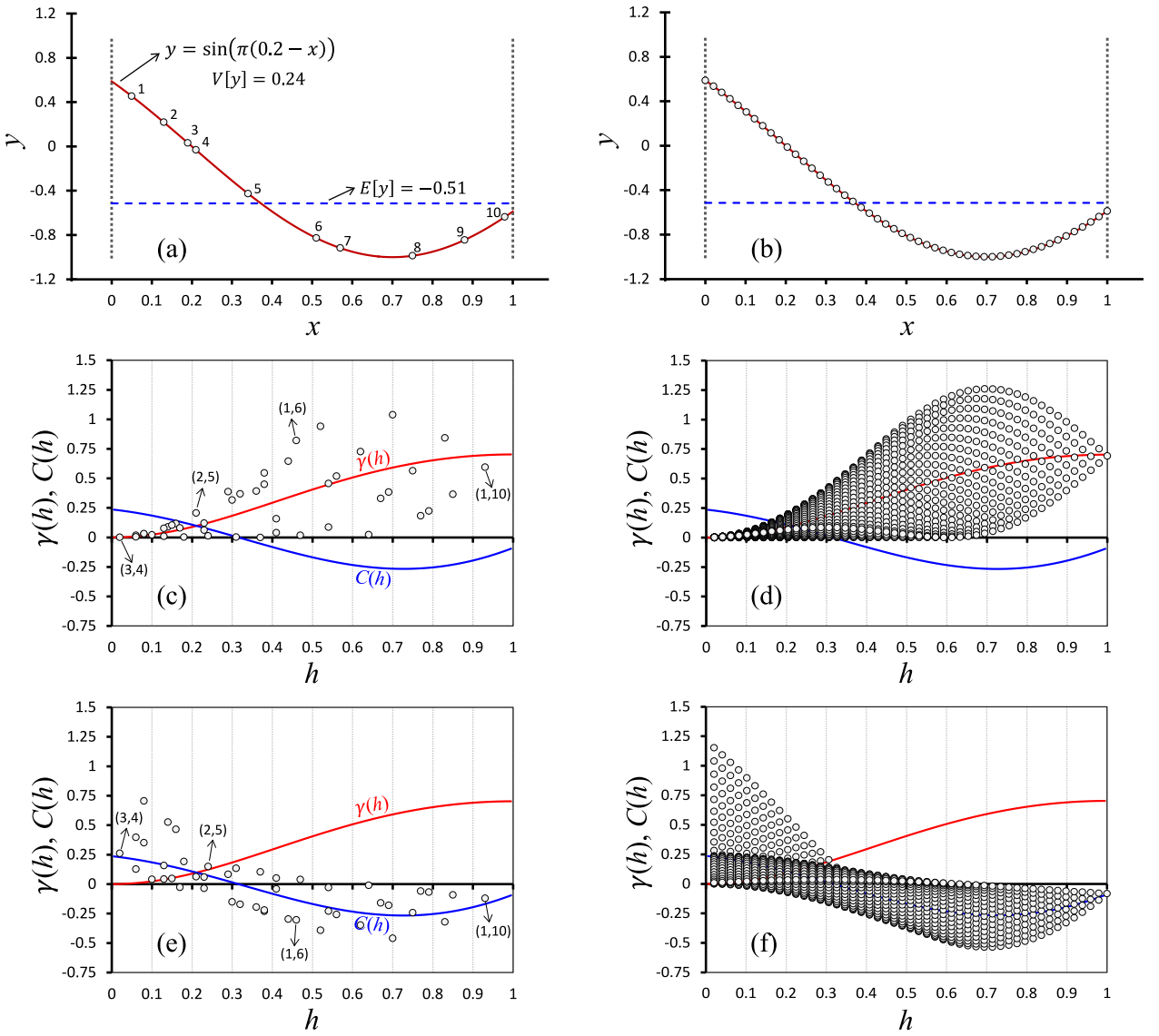


**Figure 1.** Illustration of the concept of variogram and covariogram on a hypothetical one-factor response surface shown in subplots (a) and (b). The left column relates to use of 10 randomly sampled points (see subplot a). The right column relates to use of 50 regularly sampled points (see subplot b). Subplots (c) and (d) show the corresponding values of $0.5(y(x^i) - y(x^j))^2$ for all pairs of points, $x^i$ and $x^j$ where $i$ & $j$ =1,. . ., $p$ and $p$ is the number of points. Subplots (e) and (f) show the corresponding values of $(y(x^i) - \mu_y)$ $(y(x^j) - \mu_y)$ where $\mu_y$ is the mean of the response surface. The variogram and covariogram functions shown were derived analytically.

According to these metrics, one would conclude that $f_1$ and $f_3$ are equally sensitive and slightly more sensitive than $f_2$. However, the three functions, being structurally different, have significantly different variograms (Figure 2d). Remembering that $\gamma(h)$ is a measure of "scale-dependent sensitivity," we see that functions $f_3$ and $f_1$ have similar values of $\gamma(h)$ *only* at very small values of $h$ ($\sim<0.05$), and that $f_3$ has higher values of $\gamma(h)$ for any larger $h$ (up to half of the factor range), indicating it to be the most sensitive of the three functions across all scales smaller than one. Meanwhile, $f_1$ is seen to be slightly more sensitive than $f_2$ on the scale range zero to 0.4, while $f_2$ is more sensitive on the scale range 0.4–1.

***Example 1b: Functions covering different ranges in the response.*** Figure 2e presents three functions that vary over radically different output ranges, while having constant and identical *absolute* values of the local sensitivities across the factor range (except at singular points where the derivatives change sign). All three cases have average absolute local sensitivity = $a$ (see Figure 2f), but significantly different response surface PDFs (see Figure 2g). An intuitive interpretation is that $f_1$ represents the situation with highest sensitivity of

the response $y$ to variations in factor $x$, because changes in $x$ control a larger range of the output. However, in some situations, periodicities (multimodalities) in the response surface may be very important in evaluating the impact of a factor. From the perspective of model calibration, the function $f_2$ (characterized by two distinct regions of attraction) might be deemed quite "sensitive" to $x$. Meanwhile $f_3$ is characterized by significant periodicity and has the same average absolute local sensitivity as the other two functions, but may simply represent an insensitive but nonsmooth (noisy) model response, possibly due to numerical artifacts.

The values of overall variance $V(y)$ are $\frac{a^2}{12}$, $\frac{a^2}{192}$, and $\frac{a^2}{12288}$, respectively for $f_1$, $f_2$, and $f_3$, whereas, $E\left(\left|\frac{dy}{dx}\right|\right)=a$ and $E\left(\left(\frac{dy}{dx}\right)^2\right)=a^2$ for all the three functions. Based on the Sobol approach, one would assess $f_1$ to be 16 and 1026 times more sensitive to factor $x$ than $f_2$ and $f_3$, while the Morris approach would deem the three functions to be equally sensitive.

A comparison of the variograms (Figure 2h) reveals these functions to be quite different. For $h$ values smaller than 0.01 (very small scale), the three variograms indicate almost equal sensitivity, however, for larger scales, the variogram approach agrees clearly with the Sobol approach that $f_1$ is the most sensitive. Further, the variograms of $f_2$ and $f_3$ display periodicity reflecting the multimodal structures of their respective response surfaces. Finally, the variogram of $f_3$ shows very low sensitivity across all scales, indicating *robustness* of the VARS approach against noise/roughness in the underlying response surface.

***Example 1c: Multimodal versus unimodal functions with identical variance.*** Figure 2i presents two functions having the same average local sensitivity, both equal zero (see Figure 2j). Despite having very different response surface PDFs (see Figure 2k), they have an identical overall variance $V(y)=0.11$, which runs counter to our intuitive notion of sensitivity. This happens because the variance measures overall variability of the response but is not sensitive to the *structure* of the underlying response surface—i.e., how the values of the response are organized in the factor space. Consequently, Sobol type variance-based methods are unable to take into account important structural information such as multimodality. In contrast, the Morris-based measures can differentiate between the two functions. The values of $E\left(\left|\frac{dy}{dx}\right|\right)$ for $f_1$ and $f_2$ are 1.11 and 3.01, and the corresponding values of $E\left(\left(\frac{dy}{dx}\right)^2\right)$ are 1.64 and 11.80.

This example shows nicely how a variogram conveys information about the structure of a response surface (see Figure 2l). The variogram of the multimodal function $f_2$ indicates significantly larger sensitivity for $h$ on range of zero to about 0.2. For larger scales, the variogram of $f_2$ shows periodicity caused by the multimodality of the underlying response surface. At large scales (where the difference in response surface structures becomes less significant), the variograms of $f_2$ and $f_1$ indicate somewhat similar sensitivity.

Note that in VARS, as in any variogram analysis, the maximum meaningful range of $h$ is *one half* of the factor range, because for larger $h$ values ($h > 50\%$ of the factor range), a portion of the factor range will be excluded in the calculation of $\gamma(h)$. For example, when $h$ is 50% of the factor range, in all possible pairs of points ($x^A$ and $x^B$), $x^A$ is taken from one half and $x^B$ is taken from the other half. When $h$ is 75% of the factor range, in all possible pairs of points ($x^A$ and $x^B$), $x^A$ is taken from range 0-25% and $x^B$ is taken from range 75–100%, and therefore, no points will be taken from range 25–75%.

### 2.3. Variogram Integration: A Comprehensive Metric of "Global" Sensitivity

Section 2.2 showed that the variogram of a response surface provides a sort of "spectral" representation of sensitivity across the range of possible scales. For a model with $n$ factors, a directional variogram can be constructed for each factor so that the relative sensitivity of the model response to each factor can be evaluated at any scale of interest. Accordingly, the value of $\gamma(h_i)$ at very small values of $h_i$ (say e.g., $h_i \leq 1\%$ of the factor range) represents the average small-scale (local) sensitivity of the model response to factor $i$, while at large values of $h_i$ (say e.g., $h_i =$ 25–50% of the factor range), it represents the average larger-scale sensitivity.

Except for the special case of linear models, there may not exist a single particular scale that provides an accurate assessment of sensitivity. This warrants the development of SA metrics that encompass sensitivity information over a range of scales. In VARS, such metrics of factor sensitivity can be obtained by integrating the directional variograms over some scale range of interest (equivalent to computing the cumulative area

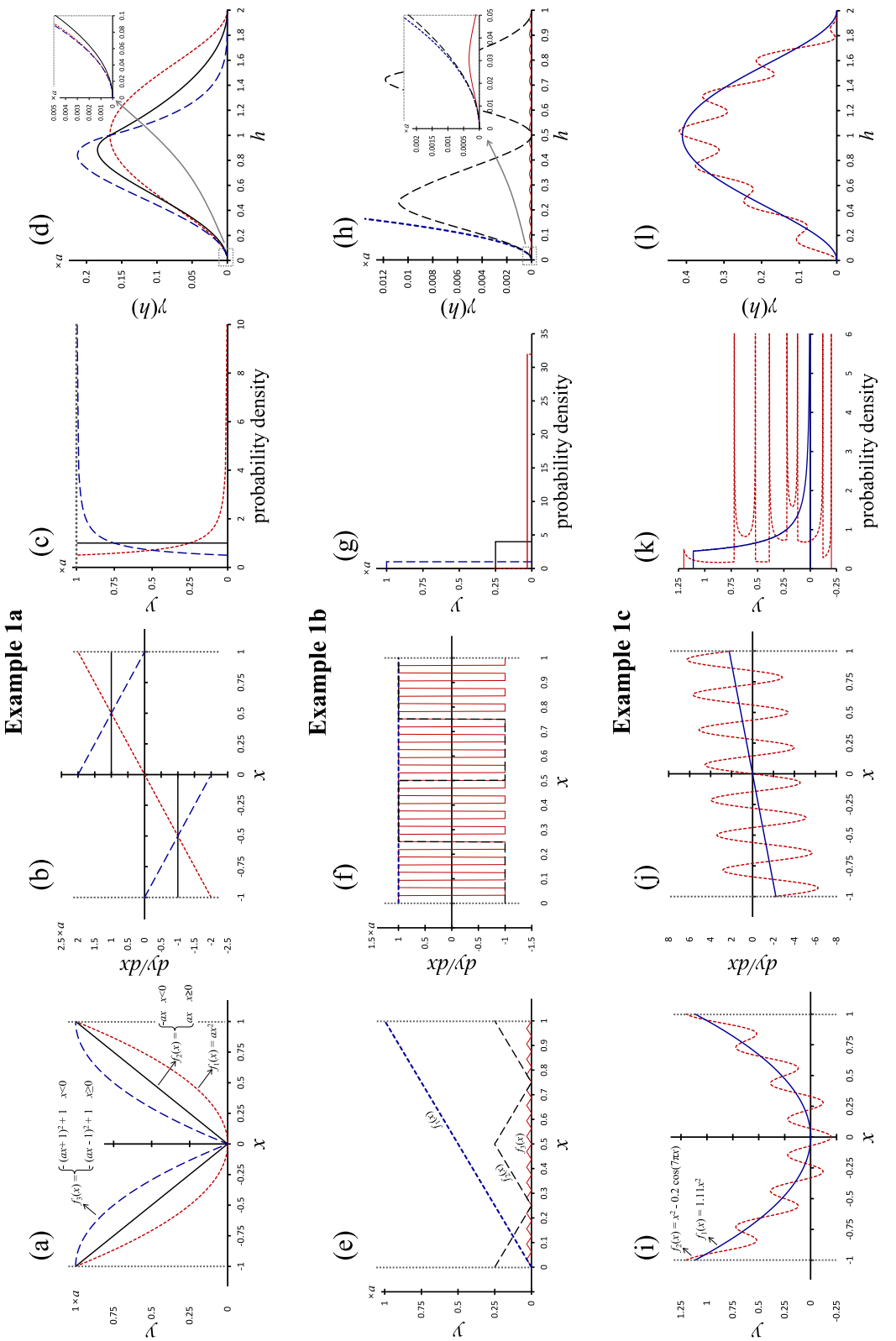


**Figure 2.** These three conceptual examples demonstrate the relationships between variograms and the assessment of sensitivity. Example 1a (first row): Three unimodal functions with different structures, but providing similar assessments for derivative-based and variance-based sensitivity measures. Example 1b (second row): three piece-wise linear functions having identical absolute slopes while covering different response ranges; these functions have identical derivative-based sensitivity but significantly different variance-based sensitivity. Example 1c (third row): A multimodal and a unimodal function having identical variance-based sensitivity but different structural organization. Subplots (a), (e), and (i) show response surfaces. Subplots (b), (f), and (j) show corresponding derivative functions. Subplots (c), (g), and (k) show corresponding probability density functions. Subplots (d), (h), and (l) show corresponding variograms. These examples show clearly that variograms can effectively differentiate between the sensitivities of the various response surfaces. Note that each of the examples can be viewed as cross sections of a multidimensional response surface having noninteracting factors; e.g., Example 1c can be viewed as cross sections of $y = 1.11\ x_1^2 + x_2^2 - 0.2\cos(7\pi x_2)$.

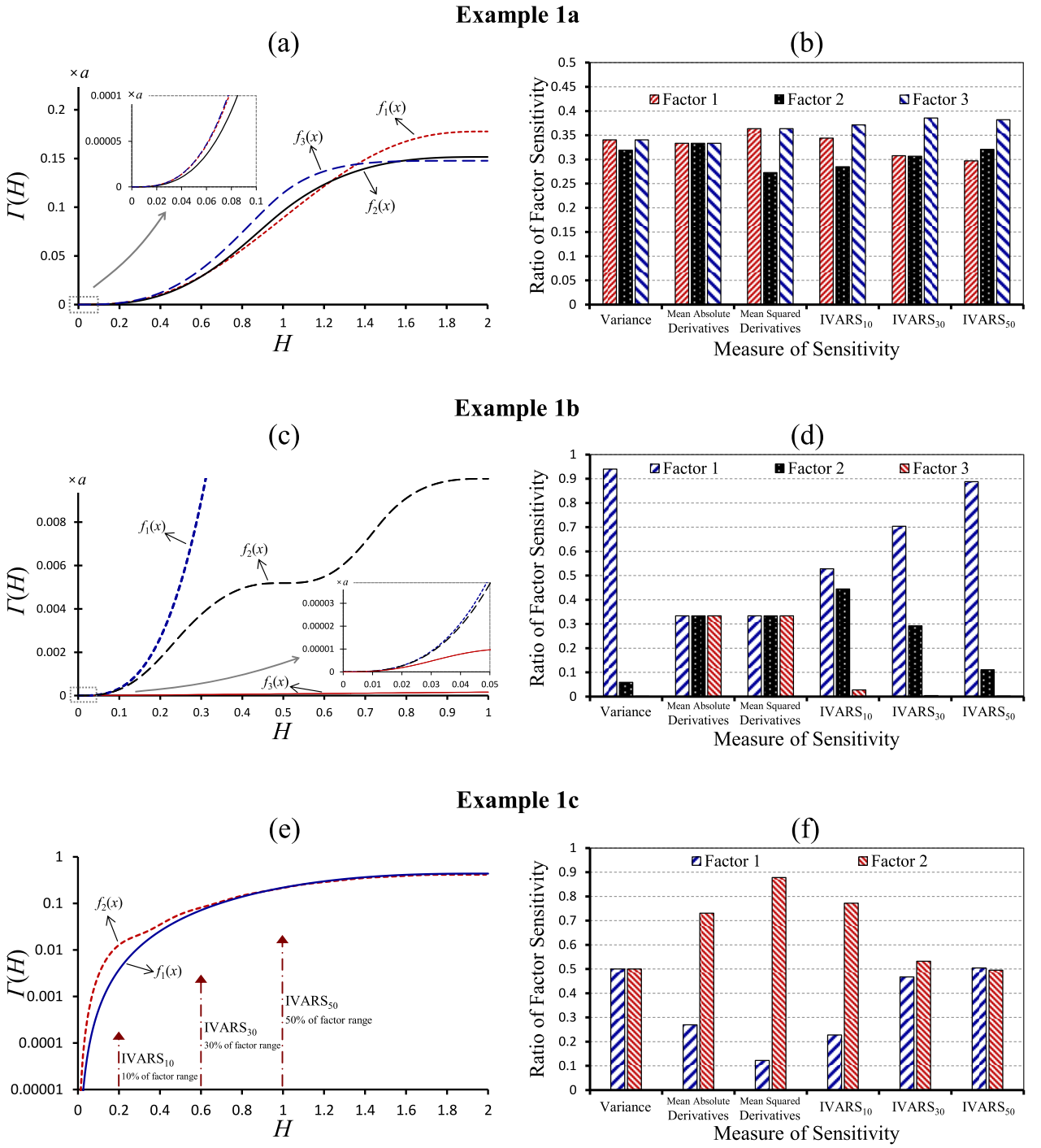


**Figure 3.** Illustration of Integrated Variograms Across a Range of Scales (IVARS). The left column (subplots a, c, and e) shows integrated variograms corresponding to the response surfaces in Example 1a, Example 1b, and Example 1c, respectively. The right column (subplots b, d, and f) shows corresponding comparisons between the IVARS metrics and the benchmark methods.

under the variogram). Given a scale range varying from zero to $H_i$ for the $i^{th}$ factor, the "Integrated Variogram," $\Gamma(H_i)$, is computed as:

$$\Gamma(H_i) = \int_0^{H_i} \gamma(h_i)\ dh_i \tag{9}$$

Figures 3a, 3c, and 3e illustrate this integrated variogram concept for the functions examined in Examples 1a, 1b, and 1c, by plotting $\Gamma(H)$ versus $H$ over the full factor range; please bear in mind that although we show $\Gamma(H)$ over the full range (for the sake of completeness), $\Gamma(H_i)$ can be meaningfully interpreted *only* when $H$ is smaller than one half of the factor range (see explanation in section 2.2). For Example 1a, $\Gamma(H)$ of $f_3$ is comparable and larger than those of $f_1$ and $f_2$ for very small $H$ values ($\sim<0.05$ equivalent to 2.5% of the factor range), while being consistently the largest for up to 50% of the factor range. Meanwhile, $f_1$ has a slightly larger $\Gamma(H)$ than $f_2$ when $H<0.5$ (0–25% of the factor range), while the converse is true when $0.5<H<1$ (0.25–50% of the factor range). For Example 1b, all the three functions have similar $\Gamma(H)$ at very small $H$ values (0–2% of the factor range), but sensitivity of the functions can be ranked as $f_1>f_2>f_3$ for any larger $H$ value. For Example 1c, the $\Gamma(H)$ is larger for $f_2$ than $f_1$ on the range $0<H<0.8$ (0–40% of the factor range), and the values become similar near $H=1$ (50% of the factor range).

These examples show that function $\Gamma(H)$, representing the "Integrated Variogram Across a Range of Scales" (IVARS) can provide a meaningful measure of the sensitivity of a model response to its factors. In each of the examples shown above, if the different functions are thought of as the responses to different (noninteracting) factors of a model, IVARS-based sensitivity measures can be used to rank the factors in terms of their influence. Based on the discussion presented above, we recommend (for example) the use of $IVARS_{10}$, $IVARS_{30}$, and $IVARS_{50}$ (computed for $H$ equal to 10%, 30%, and 50% of the factor range, respectively).

Figures 3b, 3d, and 3f show a comparison between the $IVARS_{10}$, $IVARS_{30}$, and $IVARS_{50}$ metrics of sensitivity and the Sobol and Morris-based benchmarks discussed in section 2.2.2. Each subplot shows, for one of Examples 1a–1c, the ratios of factor sensitivity (which are the values of each metric divided by the summed values of that metric over all of the factors). In Example 1a, according to all the three $IVARS_{10}$, $IVARS_{30}$, and $IVARS_{50}$ metrics, Factor 3 is the most sensitive (differing from the assessment provided by the benchmarks). Factor 1 is more sensitive than factor 2 according to $IVARS_{10}$, almost equally sensitive according to $IVARS_{30}$, and less sensitive according to $IVARS_{50}$. In Example 1b, the sensitivity ordering is factor 1 > factor 2 > factor 3 according to all the three new metrics (agreeing with the Sobol assessment). In Example 1c, factor 1 is significantly less sensitive than factor 2 according to $IVARS_{10}$ and almost equally sensitive according to $IVARS_{50}$ (agreeing with the Morris benchmark at shorter scales and the Sobol benchmark at larger scales).

## 3. Theoretical Relationship of VARS to the Morris and Sobol Methods

### 3.1. Theoretical Links to Derivative-Based SA and the Morris Method

Directional variogram $\gamma(h_i)$ of factor $i$, when $h_i$ is small relative to the factor range, can be seen to be proportional to the variance of the distribution of first-order partial derivatives in the $i$th factor direction across the space by rewriting equation (5) (multiplying both nominator and denominator inside the brackets by $h_i$) as:

$$\gamma(h_i)=\frac{1}{2}\cdot h_i{}^2 V\left(\frac{y(x_1,\ldots,x_i+h_i,\ldots,x_n)-y(x_1,\ldots,x_i,\ldots,x_n)}{h_i}\right) \tag{10}$$

and to the expectation of the distribution of the squared values of those derivatives by rewriting equation (6) as:

$$\gamma(h_i)=\frac{1}{2}\cdot h_i{}^2 E\left[\left(\frac{y(x_1,\ldots,x_i+h_i,\ldots,x_n)-y(x_1,\ldots,x_i,\ldots,x_n)}{h_i}\right)^2\right] \tag{11}$$

As the distance $h_i\to 0$, directional variogram $\gamma(h_i)$ corresponding to factor $x_i$ approaches to be $\gamma(h_i)\propto V\left(\frac{dy}{dx_i}\right) \propto E\left(\left(\frac{dy}{dx_i}\right)^2\right)$, where $V\left(\frac{dy}{dx_i}\right)=E\left(\left(\frac{dy}{dx_i}\right)^2\right)$ under the constant mean assumption presented in section 2.1. Therefore, when comparing factors $i$ and $j$, $\frac{\gamma(h_i)}{\gamma(h_j)}=V\left(\frac{dy}{dx_i}\right)\Big/V\left(\frac{dy}{dx_j}\right)=E\left(\left(\frac{dy}{dx_i}\right)^2\right)\Big/E\left(\left(\frac{dy}{dx_j}\right)^2\right)$ as $h_i$ & $h_j\to 0$. Similarly, variogram values computed for different choices for distance $h_i$ (corresponding to different finite-difference step sizes, $\Delta x$) correspond to the "elementary effects" defined in the Morris method [*Morris*, 1991]. Accordingly, the elementary effects of *Morris*, assessed at different "scales" can be seen as by-products of the VARS framework. We will, henceforth, use the acronym VARS-ACE to mean the ACtual Elementary effects across scales, the acronym VARS-ABE to mean the ABsolute Elementary effects across scales, and the acronym VARS-SQE to mean the SQuared Elementary effects across scales.

### 3.2. Theoretical Links to Variance-Based SA and the Sobol Method

For any two points in the factor space with locations $\boldsymbol{x}^A$ and $\boldsymbol{x}^B$, we have:

$$V\left(y\left(\boldsymbol{x}^A\right)-y\left(\boldsymbol{x}^B\right)\right)=V\left(y\left(\boldsymbol{x}^A\right)\right)+V\left(y\left(\boldsymbol{x}^B\right)\right)-2COV\left(y\left(\boldsymbol{x}^A\right),\ y\left(\boldsymbol{x}^B\right)\right) \tag{12}$$

Following equation (3) and (4), the above equation can be re-written as:

$$\gamma(\boldsymbol{h})=(C(\boldsymbol{0})-C(\boldsymbol{h})) \tag{13}$$

where $\boldsymbol{0}$ is an $n$-dimensional array of zeros and $C(\boldsymbol{0})=V(y(\boldsymbol{x}))$. If we have $C(\boldsymbol{h})=0$ for all values of $\boldsymbol{h}>\boldsymbol{0}$, the underlying stochastic process is characterized by a lack of spatial dependence, and the value of the variogram is constant and equal to the overall variance of the response $\gamma(\boldsymbol{h})=V(y(\boldsymbol{x}))$. Instead, if $C(\boldsymbol{h})\rightarrow 0$ as $\|\boldsymbol{h}\|\rightarrow\infty$, then $\gamma(\boldsymbol{h})\rightarrow C(\boldsymbol{0})$, where $C(\boldsymbol{0})$ is known as the variogram "sill." Accordingly, if the variogram has a sill, the value of $\gamma(\boldsymbol{h})$ at large values of $\|\boldsymbol{h}\|$ will approach the variance of the response surface.

The link to the Sobol variance-based approach now becomes clear. Each directional variogram is linked to the decomposition of response surface variance into its constituent factors. Let the set of all factors except $x_i$ be represented as $\boldsymbol{x}_{\sim i}=\{x_1,x_2,\ldots,x_{i-1},x_{i+1}\ldots,x_n\}$. The directional variogram of the $i^{\text{th}}$ factor given a specific $\boldsymbol{x}^*_{\sim i}$ (a specific cross section in the $i^{\text{th}}$ direction) in the factor space is

$$\gamma_{\boldsymbol{x}^*_{\sim i}}(h_i)=V\left(y|\boldsymbol{x}^*_{\sim i}\right)-C_{\boldsymbol{x}^*_{\sim i}}(h_i) \tag{14}$$

Taking expectation across the factor space on both sides of equation (14) results in

$$\begin{aligned} E\left[\gamma_{\boldsymbol{x}_{\sim i}}(h_i)\right]&=E[V(y|\boldsymbol{x}_{\sim i})]-E[C_{\boldsymbol{x}_{\sim i}}(h_i)]\\ \gamma(h_i)&=E[V(y|\boldsymbol{x}_{\sim i})]-E[C_{\boldsymbol{x}_{\sim i}}(h_i)]\end{aligned} \tag{15}$$

Given that the total variance of $y$, $V(y)$, can be decomposed such that

$$V(y)=V(E[y|\boldsymbol{x}_{\sim i}])+E[V(y|\boldsymbol{x}_{\sim i})] \tag{16}$$

equation (15) can be written as

$$\gamma(h_i)=S_{Ti}V(y)-E[C_{\boldsymbol{x}_{\sim i}}(h_i)] \tag{17}$$

where $S_{Ti}$ is the Sobol variance-based "total-order effect" sensitivity index of the $i^{\text{th}}$ factor. In other words, $\gamma(h_i)+E[C_{\boldsymbol{x}_{\sim i}}(h_i)]$ represents the variance contribution of the $i^{\text{th}}$ factor of any order to the total variance. Proofs of equations (14) and (16) are provided in Appendices A and B, respectively. Accordingly, variance-based total-order effects can be computed as by-products of the VARS framework—henceforth we will use the acronym VARS-TO (TO for Total Order) to refer to the TO metrics computed in this way. Section 4.1.5 of the companion paper [*Razavi and Gupta*, 2016] further illuminates this link and the implications of the constant mean assumption.

## 4. Representation of Response Surface Multimodality in VARS

While the VARS characterization of a response surface corresponds to the Morris approach at small scales and the Sobol approach at large scales, it has the important property that it characterizes the structural organization of the response surface and can, therefore, reveal a range of multimodality (or periodicity) features that may exist, from very small-scale fluctuations (e.g., noise or roughness) to large-scale (dominant) modes. Modes (non-monotonicity) in a response surface will result in negative correlations (covariance structures) and be revealed as periodicities in the variogram. This behavior is present in Examples 1a–1c at different scales (see Figure 2). In multidimensional (multifactor) problems, $\gamma_{\boldsymbol{x}^*_{\sim i}}(h_i)$, the directional variogram for factor $i$ when all other factors are fixed at $\boldsymbol{x}^*_{\sim i}$, represents the multimodalities in that cross section of the factor space (defined by $\boldsymbol{x}^*_{\sim i}$). Therefore, $\gamma(h_i)$, which is $E\left[\gamma_{\boldsymbol{x}_{\sim i}}(h_i)\right]$, averages such features for factor $i$ across the factor space and reveals the dominant ones. In spatial statistics, this behavior is known as the "hole effect"; see *Cressie* [1993] for more detail.

## 5. A Case Study: A Six-Dimensional Response Surface

Table 1 lists the different main and side VARS products used in this experiment. All of these products for a response surface are obtainable through a single VARS experiment. In the following synthetic test function

having six *fully non-interacting* factors (Example 2, as shown in Figure 4a), the function $f(.)$ is constructed as the sum of six one-factor functions, $g_1(.) \ldots, g_6(.)$, as follows:

$$y = f(x_1, \ldots, x_6) = g_1(x_1) + g_2(x_2) + \ldots + g_6(x_6) \tag{18}$$

where:

$$g_1(x_1) = -\sin(\pi x_1) - 0.3\sin(3.33\pi x_1) \tag{18a}$$

$$g_2(x_2) = -0.76\sin(\pi(x_2 - 0.2)) - 0.315 \tag{18b}$$

$$g_3(x_3) = -0.12\sin(1.05\pi(x_3 - 0.2)) - 0.02\,sin(95.24\pi x_3) - 0.96 \tag{18c}$$

$$g_4(x_4) = -0.12\sin(1.05\pi(x_4 - 0.2)) - 0.96 \tag{18d}$$

$$g_5(x_5) = -0.05\sin(\pi(x_5 - 0.2)) - 1.02 \tag{18e}$$

$$g_6(x_6) = -1.08 \tag{18f}$$

and $x_1, \ldots, x_6$ vary between zero and one. Intuitively, the sensitivity of the factors in equation (18) may be ranked as follows: $x_1 > x_2 > x_3 > x_4 > x_5 > x_6$. Comparing $x_1$ and $x_2$, the effect of $x_1$ is more complex (bi-modal), the slope along $x_1$ is generally larger, and also $x_1$ controls a larger range of variation in $y$. The effect of $x_3$ is effectively similar to the effect of $x_4$, augmented by some degree of roughness (high-frequency and low-amplitude noise). Such roughness is common in the response surfaces of EESMs. Further, the response surface formed is absolutely insensitive to $x_6$.

### 5.1. VARS Assessment of Factor Sensitivity Across Scales

Figure 4b presents the directional variograms over the full range of factor scales represented by $h_i$, $i = 1, \ldots, 6$. As shown, $\gamma(h_1) > \gamma(h_2)$ for a range of scales smaller than 0.312, and after this point $\gamma(h_1) < \gamma(h_2)$. Also, for very small scales (e.g., smaller than 0.01), $\gamma(h_3)$ is larger or as large as $\gamma(h_1)$ and $\gamma(h_2)$. For larger scales, $\gamma(h_3)$ falls behind and gradually converges to $\gamma(h_4)$. When $h_3$ and $h_4$ are exactly equal to an integer multiple of the *period of the roughness term* in $g(x_3)$, i.e., 0.021, we get $\gamma(h_3) = \gamma(h_4)$. This demonstrates the "sensitivity" of the results of a conventional sensitivity analysis procedure to the choice of scale; an issue raised by *Razavi and Gupta* [2015]. In addition, $\gamma(h_4) > \gamma(h_5)$ over the full range of scales, indicating that the response surface is more sensitive to $x_4$ than $x_5$, regardless of the choice of scale.

The integrated variograms, $\Gamma(H_1), \ldots, \Gamma(H_6)$, shown in Figure 4c provide a way of characterizing such sensitivity information over a range of scales, thereby providing a broader view of sensitivity. This is illustrated using Figure 4d, which compares the factor sensitivity ratios for four sets of sensitivity metrics obtained by the VARS framework. As there are no "interaction effects" in this case study, the variance-based (Sobol) total-order sensitivity indices (denoted as VARS-TO or Sobol-TO) are equal to the variance-based first-order sensitivity indices (denoted as Sobol-FO). The results indicate that the Sobol approach evaluates factor $x_2$ as being "more sensitive" than factor $x_1$ (more accurately stated, this means that the sensitivity of the model "response" to variations in factor $x_2$ is larger than its sensitivity to variations in factor $x_1$), which seems contrary to intuition. However, it does evaluate factor $x_3$ as being very marginally more sensitive than factor $x_4$, as the roughness term in $g(x_3)$ only very slightly inflates the variance of the function.

**Table 1.** A Summary of the VARS Products for Global Sensitivity Analysis[a]

| No. | VARS Product | Description |
|---|---|---|
| 1 | $\gamma(h)$ | Directional variogram |
| 2 | $IVARS_{10}$ | Integrated Variogram Across a Range of Scales: scale range = 0–10% |
| 3 | $IVARS_{30}$ | Integrated Variogram Across a Range of Scales: scale range = 0–30% |
| 4 | $IVARS_{50}$ | Integrated Variogram Across a Range of Scales: scale range = 0–50% |
| 5 | VARS-TO | variance-based Total-Order effect |
| 6 | VARS-ACE | mean ACtual Elementary effect across scales |
| 7 | VARS-ABE | mean ABsolute Elementary effect across scales |
| 8 | VARS-SQE | mean SQuare Elementary effect across scales |

[a]VARS-TO is effectively the same quantity as Sobol-TO (Sobol's variance-based Total-Order effect). VARS-ACE, VARS-ABE, and VARS-SQE include all variations of the Morris approach, as explained in *Razavi and Gupta* [2015], across the full range of scales (represented by step size $\Delta x$).

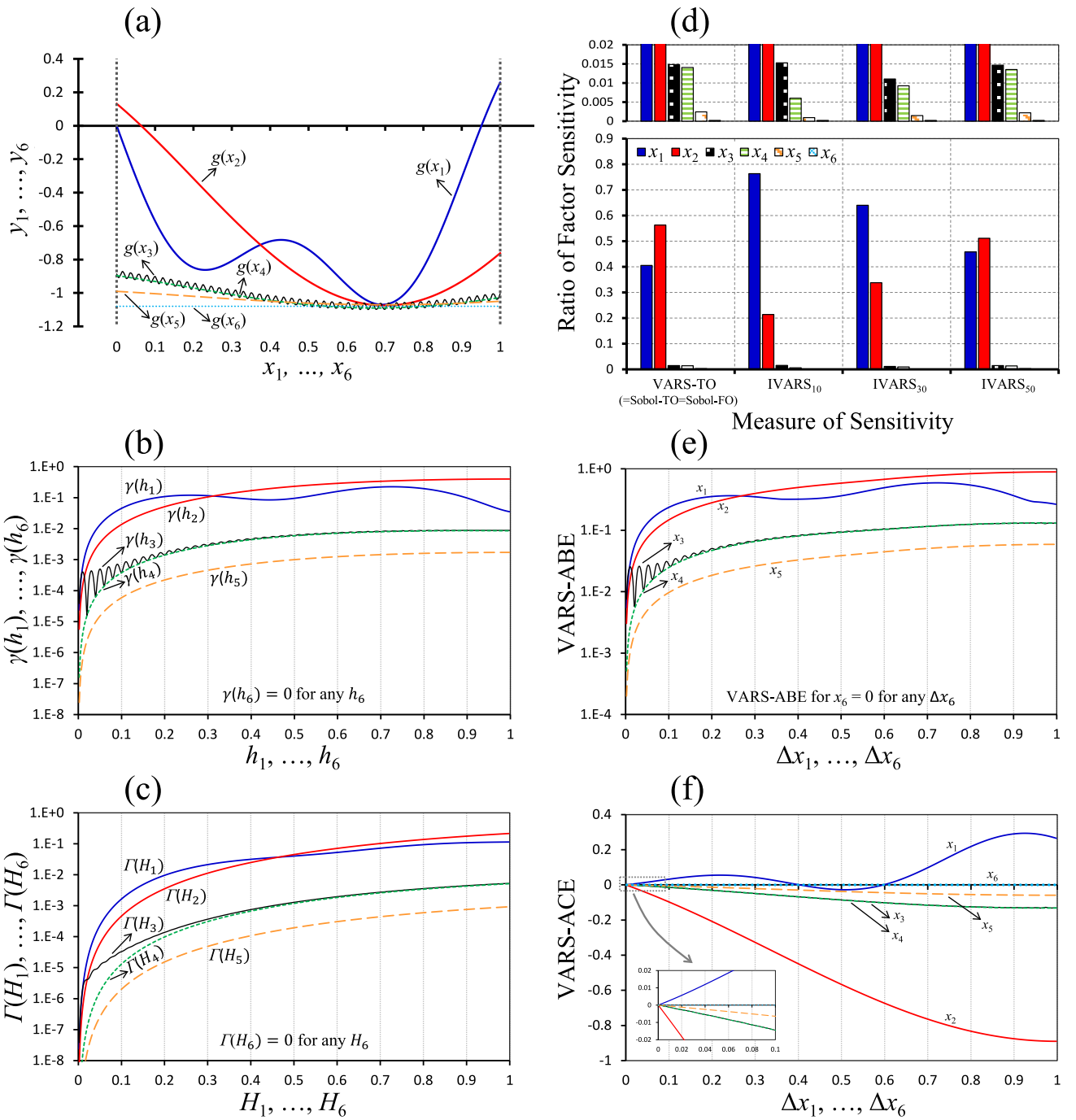


**Figure 4.** Performance of VARS on a synthetic six-factor response surface (Example 2). Subplot (a) shows the response surface, where $y = f(x_1, \ldots, x_6) = g_1(x_1) + \ldots + g_6(x_6)$. Notes: (1) there are no interactions between the factors. (2) $g_1(x_1)$ is bimodal and spans a larger response range than $g_2(x_2)$. (3) $g_3(x_3)$, which essentially is $g_4(x_4)$ augmented by noise, is intended to show how VARS characterizes noise in the response. (4) $g_5(x_5)$ and $g_6(x_6)$ are designed to show how VARS characterizes and differentiates a marginally sensitive factor versus a fully insensitive factor. (5) How VARS ranks the six factors at different scale ranges is also of interest. Subplot (b): directional variograms. Subplot (c): integrated variograms. Subplot (d): comparison of the proposed IVARS sensitivity metrics with the variance-based Total-Order effect (VARS-TO) obtained as a by-product of VARS. The top plot is a zoom-in picture of the bottom plot. VARS-TO equals the First- and Total-Order effects obtained through Sobol (Sobol-FO and Sobol-TO). Rankings based on VARS-TO and $IVARS_{50}$ are identical. Subplots (e) and (f): Mean ABsolute Elementary effects across scales (VARS-ABE) and mean ACtual Elementary effects across scales (VARS-ACE) obtained as by-products of VARS.

In contrast, the proposed $IVAR_{10}$, $IVARS_{30}$, and $IVARS_{50}$ sensitivity metrics correspond well with our intuitive understanding of sensitivity. For example, for smaller scales (represented by $IVARS_{10}$), factor $x_1$ is deemed to be significantly more sensitive than factor $x_2$, and the sensitivity to factor $x_3$ is significantly greater than that to factor $x_4$. At medium scales (represented by $IVAR_{30}$), the difference in sensitivity between factors $x_1$ and

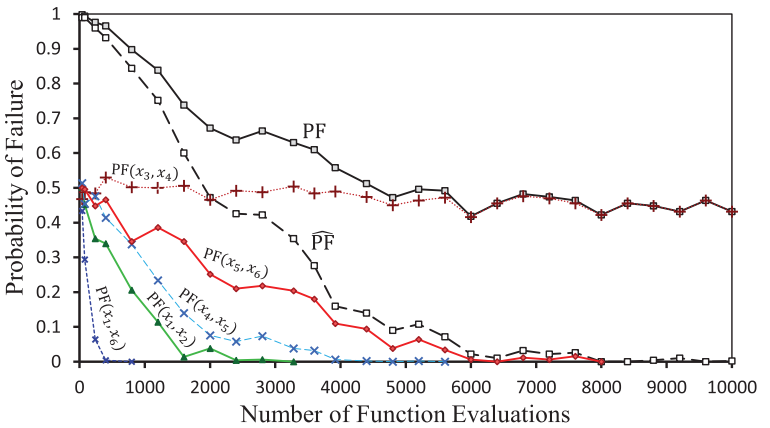


**Figure 5.** An assessment of the efficiency and reliability of the Sobol method for Example 2. The figure shows the probability of failure of the Sobol sensitivity analysis for different computational costs (i.e., numbers of function evaluations), based on the numerical implementation of *Saltelli et al.* [2008] using 500 trials (Sobol experiments) with different initial random seeds—here "failure" represents the portion of the trials that Sobol generated factor rankings inconsistent with the "true" Sobol factor ranking—PF($x_i$, $x_j$) denotes the probability of failure in correctly ranking factors $x_i$ and $x_j$ only with respect to each other − PF denotes the probability of failure in correctly ranking all the factors and $\widehat{PF}$ represents PF when ignoring the correct ranking between $x_3$ and $x_4$. For this example, VARS was able to perfectly (with probability of failure of zero) generate total-order effects (VARS-TO) using only 60 function evaluations.

$x_2$ is reduced but still significant; while for factors $x_3$ and $x_4$ the difference in sensitivity is significantly reduced. At larger scales (represented by $IVARS_{50}$), factor $x_1$ becomes slightly less sensitive than factor $x_2$, and the difference in sensitivities of factors $x_3$ and $x_4$ becomes marginal; these are consistent with the VARS-TO (=Sobol-TO) assessment of sensitivity.

Figures 4e and 4f show the VARS-ABE and VARS-ACE metrics for the six factors (equivalent to use of the Morris approach across a full range of step sizes). Since VARS-SQE is effectively equivalent to $\gamma(h_i)$ already shown in Figure 4b, it is not shown here. These figures demonstrate how implementation of the Morris approach can be sensitive to scale (the step size chosen for computing the finite-difference approximations of the derivatives). Note that VARS-ACE and VARS-ABE provide different assessments of relative factor sensitivity at different scales.

### 5.2. Numerical Implementation and Robustness

In the absence of factor interactions, VARS requires *only* one cross section along each factor direction to fully characterize all of the VARS-based sensitivity measures (which include the Sobol and Morris sensitivity measures as special cases). If we randomly pick a point along a cross section and then sample the cross section at points regularly spaced $\Delta h$ apart, we obtain $1/\Delta h$ samples of that cross section (see e.g., Figure 1b). For the results presented in section 5.1, we set $\Delta h = 0.002$ requiring a total of 3000 (= (1/0.002) * 6) function evaluations to generate results having very high precision (in practice such a small value for $\Delta h$ will not be necessary).

To evaluate robustness of the VARS approach to sampling variability, we conducted 500 independent VARS trials with $\Delta h = 0.01$, and different initial random seeds (i.e., different start points)—a total of 600 (= (1/0.01) * 6) function evaluations were required for each trial. We assess robustness by computing the "probability of failure" (PF) associated with any of the SA products (i.e., $IVARS_{10}$, $IVARS_{30}$, $IVARS_{50}$, and VARS-TO). PF is defined to represents the fractional number of trials (out of the total 500 trials) in which the factor ranking generated by a particular SA metric is not consistent with the *true* factor ranking computed using that metric in section 5.1. The resulting PF values for all of the VARS products were zero when $\Delta h = 0.01$, indicating that VARS is extremely robust and reliable.

We next repeated the experiment with a larger (more practical) value $\Delta h = 0.1$, which requires only 60 (= (1/0.1) * 6) function evaluations for each trial. In this case, PF was obtained to be zero for $IVARS_{30}$, $IVARS_{50}$, and VARS-TO, but was found to be almost 50% (PF = 0.5) for $IVARS_{10}$. To explain this, we note that $\Delta h$=0.1 is much larger than the characteristic length of the roughness existing in $g_3(x_3)$, in this

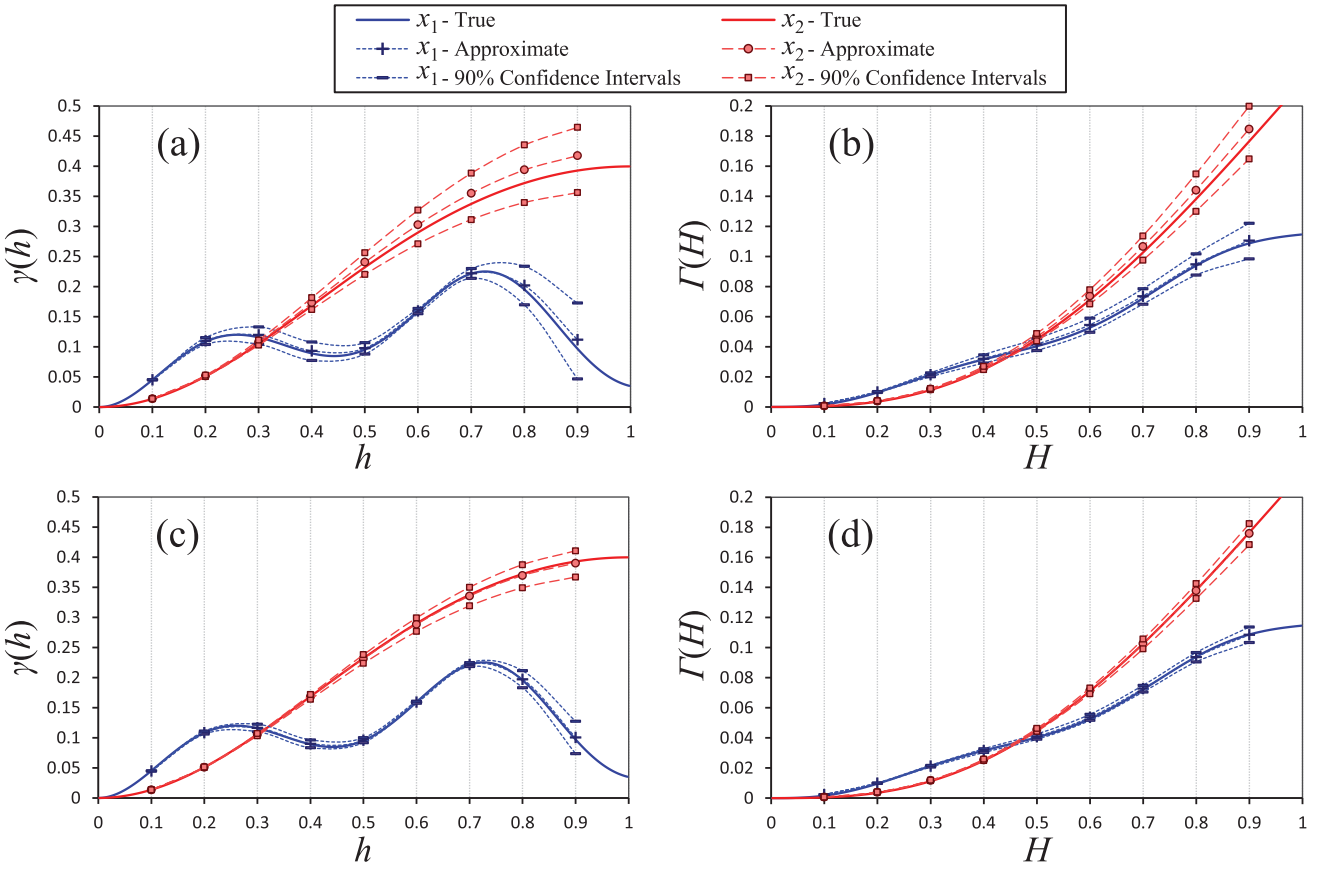


**Figure 6.** Bootstrapping of VARS on Example 2 to evaluate the uncertainty associated with VARS results. The top row corresponds to application of VARS using 10 cross sections and $\Delta h = 0.1$ (600 function evaluations). The bottom row corresponds to application of VARS using 50 cross sections and $\Delta h = 0.1$ (3000 function evaluations). Subplots (a) and (c) show variograms, while subplots (b) and (d) show integrated variograms along with their 90% bootstrap-based confidence intervals. Only the results for factors $x_1$ and $x_2$ are shown. The true variograms and integrated variograms are adapted from Figures 4b and 4c (note the change from log scale to normal scale).

case the period of the noise term. Because we are not able to characterize $\gamma(h_3)$ for $h_3 < 0.1$, and as such for $H_3 = 0.1$, we get an estimate for $\Gamma(H_3)$ that is equal to $\Gamma(H_4)$; therefore, $\text{IVARS}_{10}$ is unable to differentiate between the factor sensitivities of $x_3$ and $x_4$. Accordingly, in the 500 trials, each factor has an almost equal chance of being determined to be very marginally more sensitive than the other. Let's define $\text{PF}(x_i, x_j)$ as the probability of failure in correctly ranking factors $x_i$ and $x_j$ only with respect to each other by a sensitivity metric. Then for $\text{IVARS}_{10}$, this results in $\text{PF}(x_3, x_4) \approx 0.5$, and $\text{PF}(x_i, x_j) = 0$ for all other pairs of $x_i$ and $x_j$.

To benchmark the robustness and efficiency of the VARS framework, we also implemented the Sobol-based sampling and implementation strategy for SA as explained in *Saltelli et al.* [2008], referred to in this paper as Sobol-TO (TO for Total-Order effect). Figure 5 shows the PF values for the Sobol-TO approach (again based on 500 trials as was conducted for the VARS analysis above) for different computational costs (numbers of function evaluations). The results show that $\text{PF}(x_1, x_6)$ approaches zero after 400 function evaluations (for each random trial), indicating that to reliably differentiate a quite sensitive factor (i.e., $x_1$) from a *fully insensitive* factor (i.e., $x_6$) requires a relatively large number of function evaluations. $\text{PF}(x_5, x_6)$ approaches zero after a significantly large number ($\sim$6000) of function evaluations. Also, the method was unable to reliably differentiate between factors $x_3$ and $x_4$, even within the maximum number of function evaluations used ($\text{PF}(x_3, x_4) \approx 0.5$). Therefore, the overall result is that PF remains around 0.5 for the large computational costs. If we ignore the distinction in ranking between factors $x_3$ and $x_4$ (equivalent to ignoring the effect of the noise), and call this $\widehat{\text{PF}}$, we find that the probability of failure approaches zero after a computational cost of $\sim$6000 function evaluations. Comparing these results with those for VARS reported above, it becomes clear that the VARS approach is significantly more efficient and robust in this case—*an efficiency gain of more than two orders of magnitude* ($>$6000/60).

### 5.3. Bootstrapping to Estimate Confidence Intervals

To conclude this study, we use bootstrapping to estimate the level of confidence we can assign to the VARS results, as follows. In general, suppose we have $m$ cross sections along each factor direction. We can randomly sample with replacement $m$ of the $m$ cross sections for a large number of times, each time computing estimates of the VARS sensitivity metrics. Since in this case study there are no interactions between factors, we sample the same cross section $m$ times using different initial points and a given resolution $\Delta h$.

Figure 6 shows examples of bootstrapped confidence intervals for two independent trials of VARS using $\Delta h = 0.1$, one based on 10 samples of the cross section along each factor direction (Figures 6a and 6b) and the other one based on 50 samples of the cross section (Figures 6c and 6d). As can be seen, the 90% confidence (uncertainty) intervals are quite narrow, even for the VARS trial with only 10 samples of the cross section for each factor (with a total of 600 function evaluations), providing further evidence for the robustness of VARS against sampling variability.

## 6. Concluding Remarks

Global sensitivity analysis is a systems theoretic approach to characterizing the overall (average) sensitivity of one or more model responses across the factor space, by attributing the variability of those responses to different controlling (but uncertain) factors (e.g., model parameters, forcings, and boundary and initial conditions). This paper presents a new framework for global sensitivity analysis, referred to as *Variogram Analysis of Response Surfaces* (VARS), and provides both conceptual and theoretical explanations of why and how this framework works. The VARS framework provides a comprehensive spectrum of information about the underlying sensitivities of a response surface to its factors, while reducing to well-known and commonly used approaches to global sensitivity analysis as limiting cases. This framework is unique in that it characterizes a number of different sensitivity-related properties of response surfaces including local sensitivities and their global distribution, the global distribution of model responses, and the structural organization of the response surface (see also discussion in *Razavi and Gupta* [2015]). In particular, the VARS framework effectively tackles the scale issue of sensitivity analysis by providing sensitivity information spanning a range of scales, from small-scale features such as roughness and noise to large-scale features such as multimodality.

The framework of VARS is based on an analogy to variogram analysis, wherein *pairs* of points on the model response surface (i.e., the function mapping model factors to model responses of interest) are used to derive variogram and covariogram functions that characterize important properties of response variability in the factor space (and thereby constitute the main building blocks of VARS). "Directional" variograms and covariograms are used to quantify the *variance of change* and *covariance structure* of model response as a function of perturbation "scale" in the factor space, thereby obtaining sensitivity information across the full range of scales. While VARS provides a full spectrum of SA information (and users are encouraged to investigate this full range), we have introduced the concept of Integrated Variogram Across a Range of Scales (IVARS) to be used as a summary metric for global sensitivity.

Importantly, there is a clear theoretical link between the VARS framework and the Sobol and Morris approaches, which enables us to place the new approach in perspective while explaining how it advances the state-of-the-art of global sensitivity analysis. For practical application, a set of VARS-based sensitivity metrics can be computed, based on variogram integrations across a range of scales, which provide intuitively consistent summary metrics of global sensitivity. In addition, the framework can be used to simultaneously generate the Sobol variance-based total-order effects and the Morris derivative-based elementary effects across the full possible range of step sizes used for numerical differencing.

Notably, the VARS framework can be expected to be both computationally efficient and statistically robust, even for high-dimensional response surfaces, providing stable estimates with a relatively small number of points sampled on the response surface (i.e., a small number of model runs); this is discussed further and demonstrated in the companion paper *Razavi and Gupta* [2016]. For the simple case study presented, the VARS framework was found to be as much as two orders of magnitude more efficient than a state-of-the-art implementation of the Sobol approach. This computational efficiency is, in part, due to VARS being based on the information contained in *pairs* of points, rather than in individual points. Because a set of $k$ points sampled across a response surface results in $C_2^k$ pairs (combinations of 2 out of $k$ points), the information content grows very rapidly (the number of pairs grows as $n(nk-1)/2 \approx n^2$, where $n$ is the rate of increase

of points). So, for example if $k$=1000 points, we get 499,500 pairs but doubling ($n = 2$) the number to $k$ = 2000 points results in a fourfold ($n^2 = 4$) increase to 1,999,000 pairs.

In the companion paper, *Razavi and Gupta* [2016], we develop a sampling strategy for the application of VARS to practical problems along with a bootstrap procedure to provide estimates of confidence intervals and reliabilities of the VARS sensitivity metrics and inferred factor rankings. We also rigorously evaluate the effectiveness, efficiency, and robustness of the VAR framework for two real-data hydrological case studies having 5 and 45 parameters, respectively.

In conclusion, we hope that this new approach to sensitivity analysis will help prompt a greater level of interest in this and related issues of model development and system identification. As always we invite dialog with others interested in these and related problems. A copy of the VARS computer code can be obtained from the first author upon request for use in noncommercial applications (for commercial use please contact The University of Arizona's Tech Launch Arizona).

## Appendix A

The proof of Equation (14) is provided in the following. Consider that $\boldsymbol{x}_{\sim i}=\{x_1, x_2, \ldots, x_{i-1}, x_{i+1} \ldots, x_n\}$, which is the set of all factors except $x_i$. The directional variogram at a specific $\boldsymbol{x}^*_{\sim i}$ (i.e., a specific cross section in the $i^{\text{th}}$ direction) in the factor space is

$$\gamma_{\boldsymbol{x}^*_{\sim i}}(h_i)=\frac{1}{2}E\left[\left(y(x_i+h_i,\ \boldsymbol{x}_{\sim i})-y(x_i,\ \boldsymbol{x}_{\sim i})\right)^2|\boldsymbol{x}^*_{\sim i}\right]$$

Now within the inner brackets, add and subtract $E[y|\boldsymbol{x}_{\sim i}]$ such that

$$\gamma_{\boldsymbol{x}^*_{\sim i}}(h_i)=\frac{1}{2}E\left[\left(\left(y(x_i+h_i,\ \boldsymbol{x}_{\sim i})-E[y|\boldsymbol{x}_{\sim i}]\right)-\left(y(x_i,\ \boldsymbol{x}_{\sim i})-E[y|\boldsymbol{x}_{\sim i}]\right)\right)^2|\boldsymbol{x}^*_{\sim i}\right]$$

By squaring and simplifying, we obtain

$$\gamma_{\boldsymbol{x}^*_{\sim i}}(h_i)=\frac{1}{2}E\left[\left(\left(y(x_i+h_i,\ \boldsymbol{x}_{\sim i})-E[y|\boldsymbol{x}_{\sim i}]\right)^2+\left(y(x_i,\ \boldsymbol{x}_{\sim i})-E[y|\boldsymbol{x}_{\sim i}]\right)^2-2\left(y(x_i+h_i,\ \boldsymbol{x}_{\sim i})-E[y|\boldsymbol{x}_{\sim i}]\right)\left(y(x_i,\ \boldsymbol{x}_{\sim i})-E[y|\boldsymbol{x}_{\sim i}]\right)\right)|\boldsymbol{x}^*_{\sim i}\right]$$

$$\gamma_{\boldsymbol{x}^*_{\sim i}}(h_i)=\frac{1}{2}E\left[\left(y(x_i+h_i,\ \boldsymbol{x}_{\sim i})-E[y|\boldsymbol{x}_{\sim i}]\right)^2|\boldsymbol{x}^*_{\sim i}\right]+\frac{1}{2}E\left[\left(y(x_i,\ \boldsymbol{x}_{\sim i})-E[y|\boldsymbol{x}_{\sim i}]\right)^2|\boldsymbol{x}^*_{\sim i}\right]$$
$$-E\left[\left(y(x_i+h_i,\ \boldsymbol{x}_{\sim i})-E[y|\boldsymbol{x}_{\sim i}]\right)\left(y(x_i,\ \boldsymbol{x}_{\sim i})-E[y|\boldsymbol{x}_{\sim i}]\right)|\boldsymbol{x}^*_{\sim i}\right]$$

Each of the first two terms above is one half of variance function for the cross section and the third term is its covariance function, therefore,

$$\gamma_{\boldsymbol{x}^*_{\sim i}}(h_i)=V\left(y|\boldsymbol{x}^*_{\sim i}\right)-COV\left(y(x_i+h_i,\ x_{\sim i}), y(x_i,\ x_{\sim i})|\boldsymbol{x}^*_{\sim i}\right)$$

By using equation (4), we obtain

$$\gamma_{\boldsymbol{x}^*_{\sim i}}(h_i)=V\left(y|\boldsymbol{x}^*_{\sim i}\right)-C_{\boldsymbol{x}^*_{\sim i}}(h_i)$$

## Appendix B

The proof of Equation (16), which is called the law of total variance, is provided in the following. The variance function of $y$ can be written as

$$V(y)=E\left[\left(y-E[y]\right)^2\right]=E\left[y^2\right]-\left(E[y]\right)^2$$

According to the law of total expectation

$$V(y)=E_{\boldsymbol{x}_{\sim i}}\left[E\left[y^2|\boldsymbol{x}_{\sim i}\right]\right]-\left(E_{\boldsymbol{x}_{\sim i}}\left[E[y|\boldsymbol{x}_{\sim i}]\right]\right)^2$$

Given that $V(y|\boldsymbol{x}_{\sim i})=E[y^2|\boldsymbol{x}_{\sim i}]-\left(E[y|\boldsymbol{x}_{\sim i}]\right)^2$, we rewrite the first term and obtain:

$$V(y)=E_{\boldsymbol{x}_{\sim i}}\left[V(y|\boldsymbol{x}_{\sim i})+\left(E[y|\boldsymbol{x}_{\sim i}]\right)^2\right]-\left(E_{\boldsymbol{x}_{\sim i}}\left[E[y|\boldsymbol{x}_{\sim i}]\right]\right)^2$$

As the expectation of a sum equals the sum of expectations, we obtain

$$V(y)=E_{\boldsymbol{x}_{\sim i}}[V(y|\boldsymbol{x}_{\sim i})]+E_{\boldsymbol{x}_{\sim i}}\left[(E[y|\boldsymbol{x}_{\sim i}])^2\right]-(E_{\boldsymbol{x}_{\sim i}}[E[y|\boldsymbol{x}_{\sim i}]])^2$$

Now the second and third terms above together equal the variance of the conditional expectation, and therefore,

$$V(y)=E_{\boldsymbol{x}_{\sim i}}[V(y|\boldsymbol{x}_{\sim i})]+V_{\boldsymbol{x}_{\sim i}}\left[(E[y|\boldsymbol{x}_{\sim i}])^2\right]$$

**Acknowledgments**

The first author is thankful to the University of Saskatchewan's Global Institute for Water Security and Howard Wheater, the Canada Excellence Research Chair in Water Security, for encouragement and support. The second author received partial support from the Australian Research Council through the Centre of Excellence for Climate System Science (grant CE110001028), and from the EU-funded project "Sustainable Water Action (SWAN): Building Research Links Between EU and US" (INCO-20011-7.6 grant 294947). The data used to support this paper are synthetic and fully included in relevant sections of the paper. Interested readers may contact the first author at saman.razavi@usask.ca for more information.

## References

Campolongo, F., J. Cariboni, and A. Saltelli (2007), An effective screening design for sensitivity analysis of large models, *Environ. Modell. Software*, *22*(10), 1509–1518.

Cressie, N. A. C. (1993), *Statistics for Spatial Data*, 900 pp., John Wiley, N. Y.

Homma, T., and A. Saltelli (1996), Importance measures in global sensitivity analysis of nonlinear models, *Reliab. Eng. Syst. Safety*, *52*(1), 1–17.

Morris, M. D. (1991), Factorial sampling plans for preliminary computational experiments, *Technometrics*, *33*(2), 161–174.

Razavi, S., and H. V. Gupta (2015), What do we mean by sensitivity analysis? The need for comprehensive characterization of 'Global' sensitivity in Earth and Environmental Systems Models, *Water Resour. Res.*, *51*, 3070–3092, doi:10.1002/2014WR016527.

Razavi, S., and H. V. Gupta (2016), A new framework for comprehensive, robust, and efficient global sensitivity analysis: 2. Application, *Water Resour. Res.*, *52*, doi:10.1002/2015WR017559.

Saltelli, A., M. Ratto, T. Andres, F. Campolongo, J. Cariboni, D. Gatelli, M. Saisana, and S. Tarantola (2008), *Global Sensitivity Analysis: The Primer*, John Wiley, Hoboken, N. J.

Sobol', I. M. (1990), On sensitivity estimation for nonlinear mathematical models, *Matematicheskoe Modelirovanie*, *2*(1), pp. 112–118 [in Russian].

Sobol, I. M., and S. Kucherenko (2009), Derivative based global sensitivity measures and their link with global sensitivity indices, *Math. Comput. Simul.*, *79*(10), 3009–3017.

# A new framework for comprehensive, robust, and efficient global sensitivity analysis: 1. Theory

Razavi, Saman; Gupta, Hoshin V.

01 mingxi zhang Page 2

12/1/2024 6:41

02 mingxi zhang Page 2

12/1/2024 6:43